

Experimental Study on Reinforcement Learning-based Control of an Acrobot

Leo Dostal, Alexej Bespalko, and Daniel A. Duecker

Abstract—We present computational and experimental results on how an artificial intelligence (AI) learns to control an Acrobot using reinforcement learning (RL). Thereby the experimental setup is designed as an embedded system, which is of interest for robotics and energy harvesting applications. Specifically, we study the control of angular velocity of the Acrobot, as well as control of its total energy, which is the sum of the kinetic and the potential energy. By this means the RL algorithm is designed to drive the angular velocity or the energy of the first pendulum of the Acrobot towards a desired value. With this, libration or full rotation of the unactuated pendulum of the Acrobot is achieved. Moreover, investigations of the Acrobot control are carried out, which lead to insights about the influence of the state space discretization, the episode length, the action space or the mass of the driven pendulum on the RL control. By further numerous simulations and experiments the effects of parameter variations are evaluated.

Index Terms—Acrobot, robot control, robot learning.

I. INTRODUCTION

An essential component of conventional control technology is the derivation of a mathematical model in order to describe the real behavior of the controlled system as well as possible. The design of a controller usually goes hand in hand with complex non-linear differential equations. In practice, the involved parameters can only be determined with limited precision and usually with a lot of effort. Moreover, these parameters apply only under certain conditions. Especially the control of nonlinear underactuated systems is not easily achieved by control algorithms, if the dynamical behavior is complicated and difficult to model. For such problems finding an accurate mechanical model for a control task is often very time consuming or even not feasible. To avoid these circumstances, alternative methods from the field of machine learning may be worthwhile. Recent advances enable innovative and economical control of complex systems. Intelligent processes that were considered inefficient many years ago are now gaining new research attention and form a basis for new expanding work. This trend is strongly featured by recent advances in computing power. Hereby, especially the trend of miniaturization allows energy-efficient computing units which allow at-the-edge-computing rather than transferring data towards a server. In this sense we aim to study whether reinforcement learning based control without prior modelling of the underactuated system is possible in this context. As a particular underactuated system we use the Acrobot [1] in

our study due to the complexity of its nonlinear behavior, which makes it possible to adapt our results to various other systems in various fields, such as mechanical, MEM, robotic, and other systems. Moreover, energy generation from ocean gravity waves through pendulum excitation has become an emerging topic of interest, since one possible method of energy generation is to use gravity waves to excite the pivot of a pendulum in order to induce its oscillation or rotation [2]–[4]. Energy can be harvested from the system using electromagnetic induction. Pendulum motion control laws can be deployed in order to maximize the harvested energy. Hereby, the pendulum motion controller aims to find a policy which effectively drives the pendulum close to its eigenfrequency which maximizes the harvested energy. These are referred to as 2:1 parametric resonance – the mean period of the excitation is twice the period of the response, cf. [4]. This system can be controlled, if a second smaller pendulum is attached to the energy harvesting pendulum. The resulting system can then be identified as an Acrobot. For the Acrobot, various control strategies have been used for its control [5]–[7]. However, prior work usually focuses on the task of stabilizing the Acrobot at its inverted position, referred to as balancing control. Instead of this we aim to control the system’s energy level in the presented work *without* assuming any prior knowledge on the system itself. Thereby the control algorithms are implemented on a low cost embedded platform, which has very limited computational power. This is important for specific applications in robotics or energy harvesting. This restriction limits the possibilities of using complex control algorithms such as model predictive control. For the control of the Acrobot without prior knowledge of its model parameters and using a low power embedded platform with very limited computational power we therefore study a control strategy based on reinforcement learning (RL). Recently, RL control was adapted to the experimental setup from [8] in order to positively influence its energy state [9], by means of energy control of an Acrobot. Based on this, further investigations with the Acrobot are carried out in this study. This should lead to new insights about the influence of the state space discretization, the episode length, the action space or the mass of the driven pendulum on the RL algorithm. By further numerous simulations and experiments the effects of parameter variations are evaluated. Afterwards the combination of interesting results is presented. In this sense we study whether RL based control is feasible for energy-level control of the Acrobot.

L. Dostal, A. Bespalko, and D. A. Duecker are with Hamburg University of Technology, Institute of Mechanics and Ocean Engineering, Eissendorfer Strasse 42, 21073 Hamburg, Germany.

Corresponding author: Leo Dostal (e-mail: dostal@tuhh.de).

II. PROBLEM STATEMENT

The Acrobot is a challenging control problem in Control Theory. It is an underactuated non-linear system which consists of two links and two joints. Thereby, only the joint between the two links can be actuated by applying a torque. The system is mounted at the other joint without a possibility of actuation. The name Acrobot is a fusion of the words acrobat and robot, since the system looks like an acrobat swinging on a high bar. This robot has been also studied in the context of machine learning [5], [10]–[12].

In the right panel of Fig. 1 the Acrobot is shown, on which the experiments in this work are performed. It consists of a flywheel with the mass M and moment of inertia J_{SR} , which is mounted at the pivot in its center in such a way that it can freely rotate. At a distance l_1 from the center a servo motor including an additional weight with the mass m_M is attached, which drives a thin rod with the length l_2 and mass m_S . A point mass m_p is also located on the tip of the rod. The RL algorithm is executed on a Raspberry Pi 3 B+ with the mass m_{pi} , which has the distance l_{pi} from the pivot. Two batteries are fixed on the other two ribs of the flywheel for the power supply. These have the same distance l_A from the suspension point of the flywheel and are assumed as point masses m_A . The total center of gravity of the servo motor, the batteries and the computer is located at a distance l_{c_1} from the center of rotation, so that this setup is equivalent to a physical pendulum with the total mass $m_1 = 2m_A + m_M + m_{pi}$. Thereby, l_{c_1} is given by

$$l_{c_1} = \frac{l_1 m_M + l_{pi} m_{pi} - 2l_A m_A \sin(30)}{m_1}. \quad (1)$$

All of the above-mentioned quantities have been determined and are given in Tab I. A model of this arrangement is shown in the left panel of Fig. 1. For establishing the equations of motion, Lagrange equation of the 2nd type can be used

$$\frac{d}{dt} \frac{dL}{dq} - \frac{dL}{deq} = 0, L = T - V, \quad (2)$$

where T is the kinetic energy and V the potential energy. After the evaluation of equation (2) and the assumption of linear damping, the equations of motion for the Acrobot with actuated second arm are given by

$$\begin{aligned} (J_1 + J_2 + m_2(l_1^2 + 2l_1 l_{c_2} \cos(u)))\ddot{\theta} &= -m_2 l_{c_2} g \sin(\theta + u) \\ &- (m_1 l_{c_1} + m_2 l_1) g \sin(\theta) + m_2 l_1 l_{c_2} \sin(u) (\dot{u}^2 + 2\dot{\theta}\dot{u}) \\ &- (J_2 + m_2 l_1 l_{c_2} \cos(u))\ddot{u} - d_1 \dot{\theta}, \\ (J_2 + m_2 l_1 l_{c_2} \cos(u))\ddot{\theta} + J_2 \ddot{u} \\ &+ m_2 l_1 l_{c_2} \sin(u) \dot{\theta}^2 + m_2 g l_{c_2} \sin(\theta + u) + d_2 \dot{u} = M_u. \end{aligned} \quad (3)$$

with the angular position θ of the first pendulum, the mass $m_2 = m_s + m_p$ and angular position u of the second pendulum, damping coefficient d_1 , and acceleration due to gravity g .

In order to be able to apply energy control, we have chosen the total energy H of the first pendulum as the target energy to be reached. This energy is the sum of the kinetic and

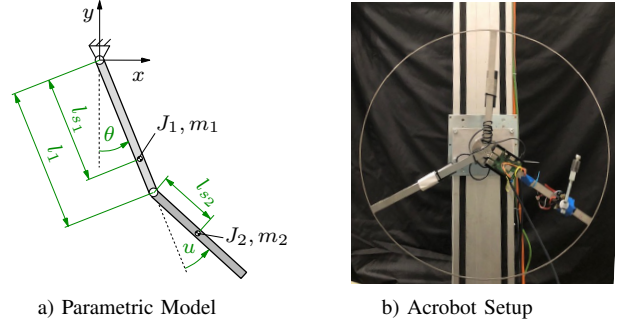


Fig. 1: Panel (a): Model of the Acrobot. Panel (b): Physical setup with RaspberryPI 3B+, IMU, and USB-powerbanks mounted on the flywheel. A video of the experimental setup can be found under: <https://youtu.be/kca-Gpdmp3I>

TABLE I: Parameters of the physical setup.

object	parameter
flywheel	$J_{SR} = 0,036 \text{ kgm}^2$
servo motor	$m_M = 0,158 \text{ kg}, l_1 = 0,26 \text{ m}$
battery cell	$m_A = 0,133 \text{ kg}, l_A = 0,15 \text{ m}$
Raspberry Pi	$m_{pi} = 0,042 \text{ kg}, l_{pi} = 0,07 \text{ m}$
small pendulum: mass	$m_p = 0,038 \text{ kg}$
small pendulum: rod	$m_r = 0,042 \text{ kg}, l_2 = 0,1 \text{ m}$

potential energy of the first pendulum, which is given by the Hamiltonian

$$H = \frac{1}{2} J_1 \dot{\theta}^2 + 2m_1 l_{c_1} g \sin^2 \left(\frac{\theta}{2} \right). \quad (4)$$

If the total energy of the full Acrobot system, which includes also the actuated second pendulum, would have been chosen as the target energy, then it would be possible to reach the target energy by just rotating the actuated second pendulum, which is simple and not of interest for us.

It is evident from Eq. (3) that the resulting nonlinear dynamics of the Acrobot are not trivial and lead to a challenging control problem, which results in a significant effort for classical controller design. This is due to the fact that a transition at a separatrix between the two different dynamical regimes of libration and rotation of the first pendulum exist, combined with highly nonlinear behavior of the system, see for example [4]. In the present work we are interested to explore whether it is possible to circumvent the derivation of equations of motion for controller development even for such difficult control problems like the present Acrobot control. For this, we use the Reinforcement Learning framework.

III. REINFORCEMENT LEARNING FRAMEWORK

In this section, we briefly recap the RL framework presented in [13] and its adaptation to pendulum energy control presented in our earlier work [9]. For the sake of brevity, we summarize the main steps of the original algorithm and point our key extensions. We refer the reader to [14], [15] for a detailed description of the underlying algorithm.

We observe that the underlying energy control problem can be written as a Markov decision process (MDP) consisting of discrete states S , actions A , an energy-based rewards function

$R(s, a)$, and a state transition matrix $P(s'|s, a)$. This transition probability matrix represents the algorithm's belief on the expected successor state s' given the current state $s \in S$ and an selected action $a \in A$. Therefore, the RL-algorithm chooses a based on the reward function.

We define a value function $v(s)$ which determines the value of the single state s . Moreover, the state-action value function $q(a, s)$ describes the value of the corresponding state-action pair. Note that our goal is to find the optimal state-action value function $q^*(s, a)$. This, can be determined via iterating over the Bellmann equation. Hence, the optimal policy $\pi(s)$ can be obtained from

$$\pi(s) = \arg \min_a q^*(s, a). \quad (5)$$

Initially, the model is unknown to the RL-algorithm. Thus, a fundamental trade-off arises between gathering system information to find good actions (*exploration*) and the selection of good actions which drive the system to the desired goal (*exploitation*). This is done in an iterative manner as we update parameters and evaluate the policy at the end of each episode.

The state-space S is discretized into states consisting of intervals of the Acrobot's angular position θ and its angular velocity $\dot{\theta}$.

Note that at a first glance, a finer state discretization is likely to improve the algorithm's performance. However, this becomes challenging for two reasons: First, the algorithm require additional the efforts for system model exploration, as revisiting of states becomes less likely. Second, deployment on embedded hardware likely renders infeasible due to its very limited computational power data storage.

In order to keep the algorithm simple our action space A only consists of two actions. Hereby, applying a_1 results in a counter clockwise motion of the actuated lever and a_2 results in a clockwise motion. This leads to an increase and decrease of the lever angle $u \in [\pi/2, 3\pi/2]$, respectively.

We design the rewards function such that it punishes deviation between the first pendulum's energy level Eq. (4) and the desired energy level H_d reading

$$R(s', a) = -(H - H_d)^2. \quad (6)$$

Hereby, we weigh larger deviations from the nominal value stronger, note the square in Eq. (6). By solving for $H(\theta, \dot{\theta})$, the reward received can be converted back into the current energy level H . If the terminal state s_T is reached, a high negative reward is assigned in order to penalize control leading out of the discretized region. Consider the general case of the Acrobot's parameters, such as I_1, l_1 , etc., being unknown. Hereby, it is appealing to use the generic scaled energy \tilde{H} , within the reward function,

$$\tilde{H} = \frac{1}{2}\dot{\theta}^2 + c_{\text{exp}} 2 \sin^2 \left(\frac{\theta}{2} \right), \quad (7)$$

where \tilde{H} is proportional to the energy H . Note that, the coefficient c_{exp} has to be identified experimentally which is described in the following. First, the Acrobot is started at an arbitrary angle θ_s . This leads to an oscillating but non rotating motion of the Acrobot. We measure the angle θ_{meas} when the

angular velocity $\dot{\theta}$ equals zero. Second, we measure $\dot{\theta}_{\text{meas}}$ at $\theta = 0$. The measured values are substituted into Eq. (7), such that

$$\tilde{H}(0, \dot{\theta}_{\text{meas}}) = \frac{1}{2}\dot{\theta}_{\text{meas}}^2 \quad (8)$$

and

$$\tilde{H}(\theta_{\text{meas}}, 0) = c_{\text{exp}} 2 \sin^2 \left(\frac{\theta_{\text{meas}}}{2} \right). \quad (9)$$

Since the energy $\tilde{H}(\theta, \dot{\theta})$ is expected to be constant we get

$$\tilde{H}(0, \dot{\theta}) = \tilde{H}(\theta, 0). \quad (10)$$

Substituting Eq. (8) and (9) into Eq. (10) we get

$$c_{\text{exp}} = \frac{\frac{1}{2}\dot{\theta}_{\text{meas}}^2}{2 \sin^2 \left(\frac{1}{2}\theta_{\text{meas}} \right)}. \quad (11)$$

We find it straight forward to determine the energy \tilde{H}_{θ_0} in a calibration step by starting at the angle θ_0 and angular velocity $\dot{\theta}_0 = 0$, followed by measuring $\dot{\theta}_{\text{cal}}$ at $\theta = 0$. Hence,

$$\tilde{H}_{\theta_0} = \frac{1}{2}\dot{\theta}_{\text{cal}}^2. \quad (12)$$

As discussed before, the RL-algorithm runs in episodes. An episode are terminated if either the terminal state or the maximum episode length is reached. At the beginning of each episode, the algorithm determines its current state s by measuring the angle θ and the angular velocity $\dot{\theta}$.

Note that the state space is discrete. Thus, applying action a may or may not change the system state. In any case we obtain the successor state s' as before from new measurements of θ and $\dot{\theta}$ respectively. This is conveniently done at the next episode's time step and we give the corresponding reward $R(s', a)$ to the algorithm and s' becomes s of the new time step.

The action selection is performed based on the current state s , the transition probability matrix $P(s'|s, a)$ and the state reward matrix $R(s, a)$. Hereby, an action a_i is favored based on the expected reward $R(s, a_i)$ given the current dynamics belief $P(s'|s, a)$. However, beside the direct next state action selection affects the gathering of potential future rewards given this state. These potential rewards are captured by the state value $v(s)$. Anyhow, since we prefer rewards gained in the near future over long-term gains we discount future rewards by a depreciation factor γ . Revisiting the trade-off between exploration and exploitation, the action selection is altered with a probability p_{explore} to enforce an exploration of the surrounding state space even at later episodes. Note that since the algorithm has no prior knowledge on the system dynamics, altering the selected action is an important aspect in order to expand the validity of the dynamics model $P(s'|s, a)$ within the whole state space.

Within a single episode all state transitions, actions and their corresponding rewards are logged. When the episode is terminated, the value function $v(s)$, the state reward matrix $R(s, a)$, and the state transition matrix $P(s'|s, a)$ are update accordingly to the logged state transitions. Finally, the next episode is initialized.

At the terminus of episode k , policy iteration is performed to compute an improved state value function $v_{k+1}(s)$ for the

subsequent episode. Therefore, the improved dynamics model from the previous step allows for a more accurate prediction of each state's successor state. Thus, the prediction of the corresponding expected rewards can be improved. This leads to a fast convergence towards an optimal policy over the subsequent episodes.

IV. SIMULATION

In order to examine the RL controller, we use the simplifying assumptions $l_{c_1} = l_1$, $l_{c_2} = l_2$, and the moments of inertia $I_1 = m_1 l_1^2$ and $I_2 = m_2 l_2^2$. The basic parameter values of the Acrobot are set to $d_1 = 0.08$ Nms, $l_1 = 4$ m, $l_2 = 1.3$ m, and $m_1 = 2$ kg for the simulation of the RL controller introduced in Sec. III.

We define an initial configuration (ICO) as performance baseline for the following simulation analysis:

Performance Baseline Setup ICO

- The angle $\theta \in [0^\circ, 360^\circ]$ is discretized into 36 angular positions with the angular increment being $\Delta\theta = 10^\circ$. The angular velocity $\dot{\theta} \in [-5.5]$ rad/s is discretized into 40 elements with step size $\Delta\dot{\theta} = 0.25$ rad/s. The state space consists of the product of these two sets and an additional terminal state s_T , representing all states outside this set.
- The number of episodes in the learning phase is set to 300. Hereby, the episode length is 1000s using the discretization $\Delta t_{\text{sim}} = 10$ ms
- Mass of the actuated pendulum is set to $m_2 = 2$ kg
- In each time step one of two possible actions $a \in \mathcal{A} = \{a_1 = \text{'negative angle step'}, a_2 = \text{'positive angle step'}\}$ can be selected.
- We use the reward function Eq. (6). Hereby, we set the desired energy level of the first pendulum to $H_d = 1.3g/l_1$, which is close to the energy level of the separatrix. Without the second pendulum, the separatrix is located at $H_s = 2\alpha$.

We are interested in the question of whether the RL controller is capable of learning the rather complicated nonlinear dynamical behavior resulting from the equation of motion (3), while actuating only the small second pendulum.

The simulation results for the ICO in Fig. 2 show the energy evolution at episodes 1, 100, and 300, starting at a low randomly chosen initial energy. It can be clearly seen, that the RL controller is capable to learn a policy which maintains the energy of the first pendulum close to a desired energy level. The value function determined by the RL controller is depicted in Fig. 3, which closely resembles the nonlinear structure of the most valuable states close to the desired energy level H_d . The convergence towards the optimal policy is indicated by the convergence of the mean energy of the first pendulum to the desired energy H_d , which was calculated from 10 learning runs, see Fig. 4. The non-monotonic convergence is caused by leaving the angular velocity region $\dot{\theta} \in [-5, 5]$ rad/s and restarting the pendulum at zero energy.

The corresponding ICO learning curve (LC_{ICO}) is depicted in Fig. 5. The learning curve reflects the average reward received according to Eq. (6) within each episode. It is obvious,

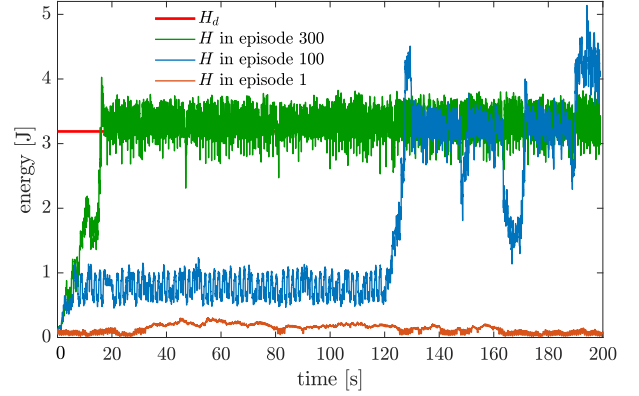


Fig. 2: Energy of the first pendulum episode 1, 100, and 300.

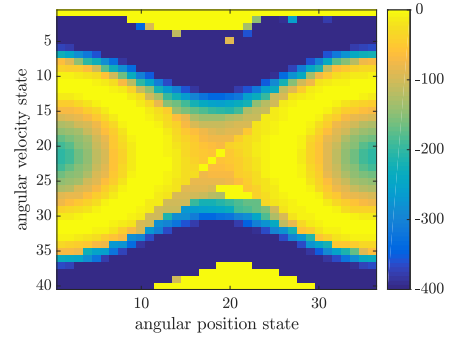


Fig. 3: Value function obtained from 300 policy iterations.

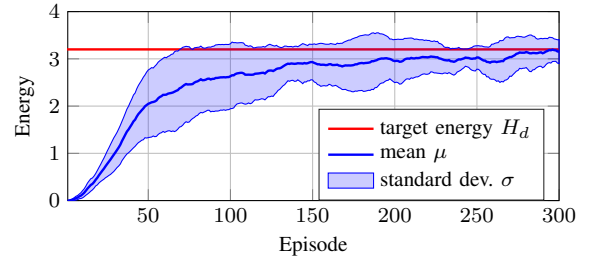


Fig. 4: Energy H averaged over 10 runs.

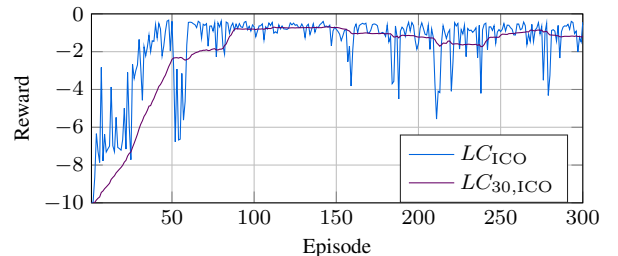


Fig. 5: Best result for 10 simulation runs using the ICO.

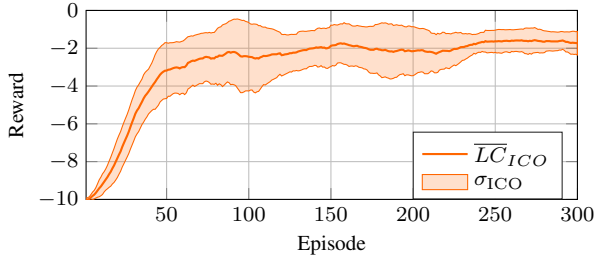


Fig. 6: The summarized result for 10 independent simulations of the RL controller using the ICO.

that the learning curve can never reach a value higher than zero. The performance of the RL-controller increases with higher values of the learning curve. Therefore, we will mostly use the learning curves in the following in order to analyze the performance of the various RL-controller setups.

In this example, the values from the 100th episode onward have small fluctuations with occasional stronger outliers. These are often caused by the exploration probability of 10%, in order that the controller can explore the state space. Such outliers and fluctuations of high frequency are obstructive for comparison with other learning curves. Therefore, the data is low-pass filtered by forming the so-called moving average over thirty episodes (LC_{30}). The result can be seen in Fig. 5.

Note that, all learning curves will differ from each other due to their statistical character. Therefore, ten simulations are performed and the corresponding mean value (\overline{LC}), as well as the standard deviation σ_{ICO} are determined. The results for the ICO are summarized in Fig. 6.

Ideally, after a sufficiently long learning period the mean values move towards the zero line, while the standard deviation remains as small as possible. In addition, the unfiltered learning curves should not show strong fluctuations.

V. STUDY AND IMPROVEMENT OF RL CONTROLLER USING SIMULATION

In order to improve the energy stabilizing RL controller for the Acrobot, we analyze the influence of state space discretization, modification of the action space, the episode length, and the mass of the actuated pendulum on the performance of the RL controller in the simulation.

A. State space discretization

One might intuitively assume that learning will be improved when choosing smaller state discretizations. However, fine discretizations require larger sets of training data in order to infer a robust policy. Moreover, depending on the actual problem the limited memory and processor power might render this option infeasible.

Let the state space be defined by $\mathcal{S} = \mathcal{S}_1 \times \mathcal{S}_2 \cup s_T$, where \mathcal{S}_1 and \mathcal{S}_2 contain the discrete angular positions and discrete angular velocities respectively and s_T is the terminal state. Both sets \mathcal{S}_1 and \mathcal{S}_2 can be either reduced, increased, or left unchanged within the same state limits. This corresponds to 3^2 combinatorial possibilities of changing the state space by an alternative choice of step sizes. Since there exist also infinite

TABLE II: Selected alternative state discretizations.

Case	State Discretization	States $ \mathcal{S} $
ICO	$\Delta\theta = 10^\circ, \Delta\dot{\theta} = 0,25 \text{ rad/s}$	1441
1	$\Delta\theta = 8^\circ, \Delta\dot{\theta} = 0,25 \text{ rad/s}$	1801
2	$\Delta\theta = 5^\circ, \Delta\dot{\theta} = 0,25 \text{ rad/s}$	2881
3	$\Delta\theta = 10^\circ, \Delta\dot{\theta} = 0,2 \text{ rad/s}$	1801
4	$\Delta\theta = 10^\circ, \Delta\dot{\theta} = 0,1 \text{ rad/s}$	3601
5	$\Delta\theta = 8^\circ, \Delta\dot{\theta} = 0,2 \text{ rad/s}$	2251
6	$\Delta\theta = 5^\circ, \Delta\dot{\theta} = 0,1 \text{ rad/s}$	7201
7	$\Delta\theta = 12^\circ, \Delta\dot{\theta} = 0,3125 \text{ rad/s}$	961
8	$\Delta\theta = 20^\circ, \Delta\dot{\theta} = 0,5 \text{ rad/s}$	361
9	$\Delta\theta = 12^\circ, \Delta\dot{\theta} = 0,25 \text{ rad/s}$	1201
10	$\Delta\theta = 20^\circ, \Delta\dot{\theta} = 0,25 \text{ rad/s}$	721
11	$\Delta\theta = 10^\circ, \Delta\dot{\theta} = 0,3125 \text{ rad/s}$	1153
12	$\Delta\theta = 10^\circ, \Delta\dot{\theta} = 0,5 \text{ rad/s}$	721

possibilities to choose the sampling intervals, we limit our study to 12 configurations which are summarized in Tab. II.

The results for cases 1 to 12 are depicted in Fig. 7. Note that the last index denotes the corresponding case number, such as $LC_{30,1}$ for the learning curve of case 1, which is averaged over 30 episodes. Reducing the step size from 10° to 8° qualitatively worsens the result with respect to the ICO-baseline from Fig. 6. Smaller rewards are achieved and the average values fluctuate comparatively strongly. Halving the step size to $\Delta\theta = 5^\circ$ reduces the reward even more.

The red curve for case 4 reaches a reward value of -4 and the large standard deviation is clearly visible. The curve for case 3, on the other hand, performs much better between episodes 100 and 200. The standard deviation gradually decreases and the curve of the corresponding mean moves into the interval $[-2, -1]$.

For cases 5 and 6, we reduce the discretization for both states, which leads to a less pronounced initial learning phase. In addition, the mean values become smaller and smaller with increasing refinement of the state space. Apparently the state space cannot be sufficiently explored due to its size. As a consequence, the quality of the learned policy decreases.

Cases 7 and 8 consider the scenario of a slight increase of $\Delta\theta$ and $\Delta\dot{\theta}$. After about 100 episodes, the curve for case 7 lies mostly below the value of -2 and gets lower than the curve for case 8 towards the end. Furthermore, the graph for case 7 shows a notable behaviour of the standard deviation, as it increases strongly towards the end.

Case 8 considers a strong reduction of the state space from 1441 to 361 states.

For this case, large fluctuations in the first half of the learning period can be observed. Nevertheless, these fluctuations are reduced and the mean value approaches the zero line.

From cases 9 and 10 it can be seen that changes of the step size $\Delta\theta$ affect the results only slightly, since the corresponding mean values, as well as the standard deviations are quite similar. The mean values remain within the interval $[-4, -2]$ and the standard deviations increase towards the end. Case 11 and 12 led to the best obtained learning curves in the simulations. One of these learning curves is shown in Fig. 8. There, the values remain near zero from episode 200

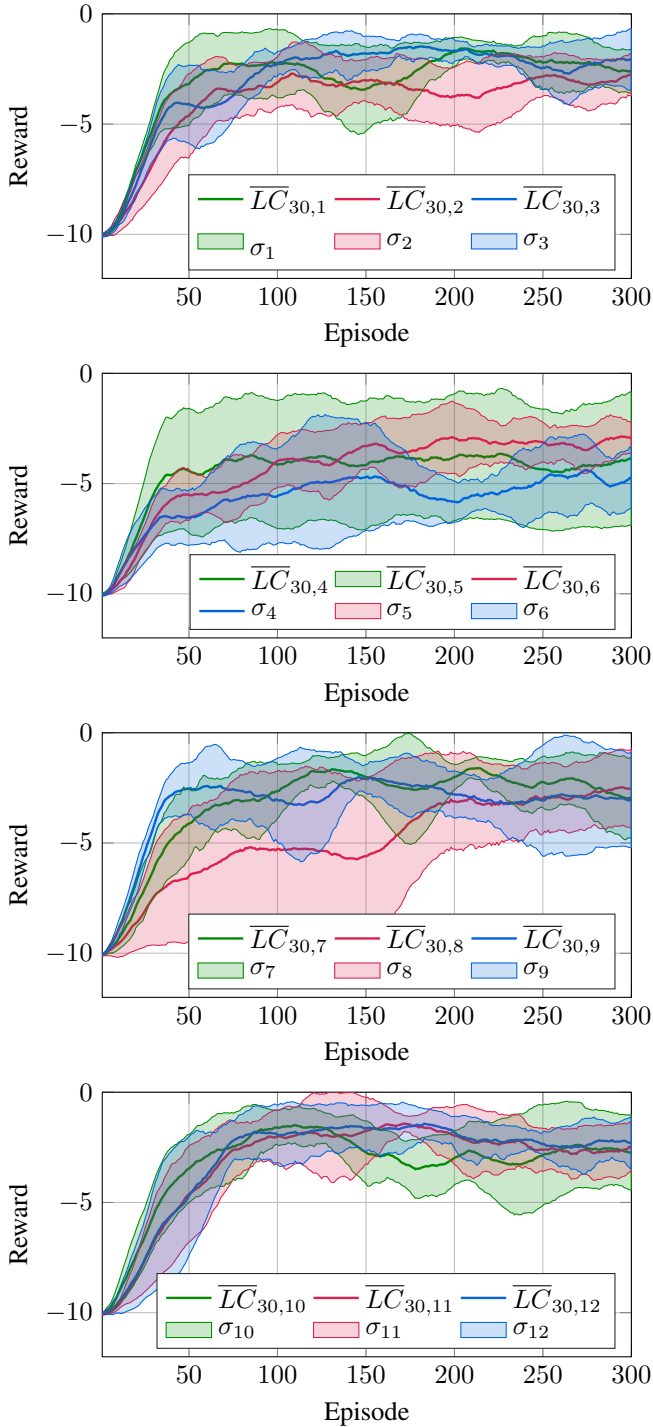


Fig. 7: Summarized results for cases 1 to 12.

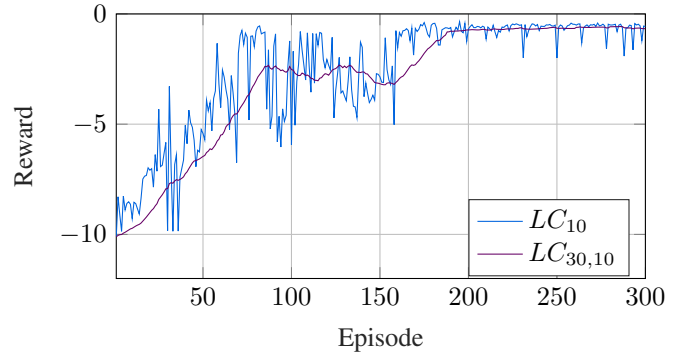


Fig. 8: Best learning curve for case 11.

with smallest fluctuations. Apart from a few small peaks, the original curve almost coincides with the sliding average.

In comparison to the baseline ICO configuration, the scattering at the beginning of the learning phase is higher. The curves for cases 11 and 12 have a almost identical quality. The doubling of the step size even caused an improvement. Therefore, this case was also tested in the experiment, as can be seen in section VII.

In summary, cases 9-12 show that, although the RL algorithm faced a strong reduction of the state space, a good control policies can still be found. In contrast, the analysis of setups with finer discretization showed rather negative tendencies except for case 3. However, the result might differ when longer episodes are considered.

B. Length of the episodes

The longer the episode length the more data is available to infer a control policy from. On an intuitive basis, the controller requires enough time to, first, explore the system dynamics and than, second, exploit this knowledge within its control policy. In order to identify trends, we run simulations using the test cases from Tab. III.

Note that the total learning time remains constant with a total of 300000s. As a result, the total number of episodes and thus the number of strategy optimizations varies.

Fig. 9 illustrates the development when the episode length is changed according to Tab. III.

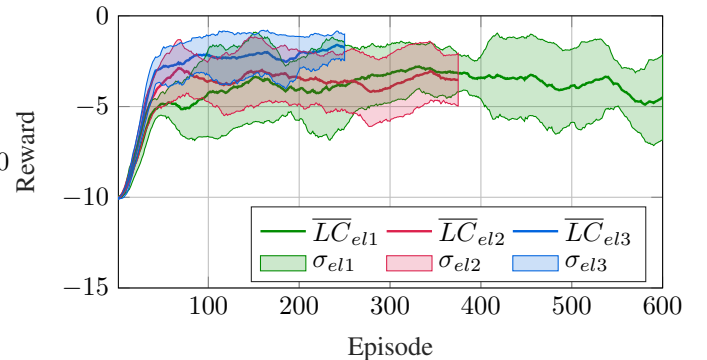


Fig. 9: Summarized results: Case $el1$ to case $el3$.

TABLE III: Selected alternatives for changing the episode length.

case	time steps
ICO	100,000
el1	50,000
el2	80,000
el3	120,000
el4	200,000

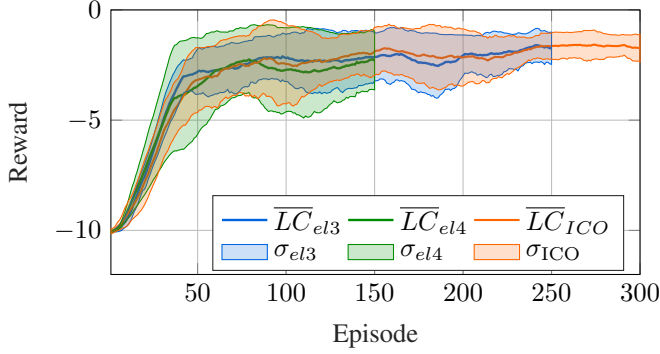


Fig. 10: Summarized results: Case *el3*, case *el4*, and *ICO*.

For the case *el1* with halved number of time steps compared to the *ICO*, the mean values are lower and show a more irregular behavior. This is due to the fact that the training of the swing-up phase dominates in this case, but keeping the energy at the desired energy level is less trained. If the episode length is shortened by 20,000 time steps (case *el2*), the mean value still remains below -2 , but the curve shows less variation. The overall result improves not significantly if the episode length of the *ICO* is extended by 20,000 time steps, which is case *el3*, as can be observed in Fig. 10.

Thus, we see that after the learning period's half-time the average reward shows a relatively smooth behaviour. Moreover, there are no more outliers. From episode 80 onwards, the moving average runs almost horizontally and close to the zero target line. This means that including additional episodes will probably only smooth the original curve.

However, the overall results including the cases *el3* and *el4* are worse than the *ICO*-baseline, as can be seen in Fig. 10. Since the total learning time remains the same, the controller can only swing up 150 times in case *el4* or 250 times in case *el3* instead of 300 times compared to the *ICO* and the swing-up strategy is therefore less often trained.

In conclusion longer episodes result in a relatively longer time spent within the stabilization phase. In contrast, short episodes support learning of the swing-up phase. In the *ICO* setup these phases are already well balanced.

C. Augmented action space

So far, the RL algorithm only considers two actions. While an actuation with a larger angular amplitude of the second pendulum is advantageous in the swing-up phase, a small amplitude or even no action might be beneficial to stabilize the Acrobot at the desired energy level. Therefore, the action space

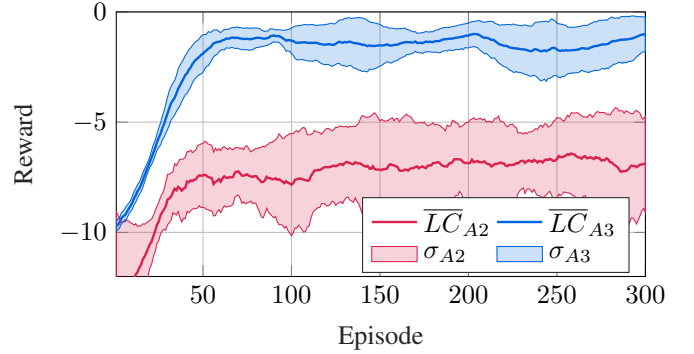


Fig. 11: Learning curves for the action sets $\mathcal{A}_2 = \{a_1, a_2, a_3\}$ and $\mathcal{A}_3 = \{a_3, a_4, a_5\}$.

is augmented by additional action states in order to explore possible positive impacts on the optimized control policy.

We introduce the following actions: $a_3 =$ 'do nothing', $a_1 =$ 'negative angle step', $a_2 =$ 'positive angle step', $a_4 =$ 'minimum angle', $a_5 =$ 'maximum angle'. An early testing showed that an augmentation with all five actions at the same time considerably decreases the control performance. This is likely because the RL controller is not able to explore the Acrobot dynamics sufficiently, as it faces too many possible actions for the given constant learning time. Due to the increase of action states, the transition matrix $\mathbf{P}(s'|s, a)$ increases and thus the training data needed to learn the state transition sufficiently. As a result, the size of the action space should remain as small as possible. Hence, we examine the following reduced action space configurations: $\mathcal{A}_1 = \{a_4, a_5\}$, $\mathcal{A}_2 = \{a_3, a_4, a_5\}$ and $\mathcal{A}_3 = \{a_1, a_2, a_3\}$.

Note that the action space remains the same in both phases, the swing-up and the stabilization phase. This enforces that the finally selected action set serves as a good compromise for both control phases.

The simulation runs using action set \mathcal{A}_1 do not achieve satisfactory performance. The controller can not keep the deviation from the target value within satisfactory limits. Using the set \mathcal{A}_2 and \mathcal{A}_3 including the action $a_3 =$ 'do nothing', the learning curves depicted in Fig. 11 were achieved.

Obviously, using set \mathcal{A}_2 the learning process is considerably worse compared to the use of the *ICO*. For the case \mathcal{A}_3 , which is the *ICO* action space is expanded with action a_3 , a positive effect on the learning curve is observed.

The $\overline{LC}_{\mathcal{A}_3}$ -curve is above the value -2 while its standard deviation is comparatively small. Compared to the learning curve from Fig. 5 the initial learning phase can be seen as already completed after about 40 episodes.

D. Mass of the actuated pendulum.

The servo actuator of the second pendulum influences the kinetic and potential energy of the overall system. In the experiment, the servo motor has a limited actuating torque, which can be applied in an on/off-fashion. Thus, it is the maximum for each action. If the mass is increased, the maximum angular acceleration \ddot{u} decreases accordingly due to the mass inertia. In the simulation, however, the dynamics

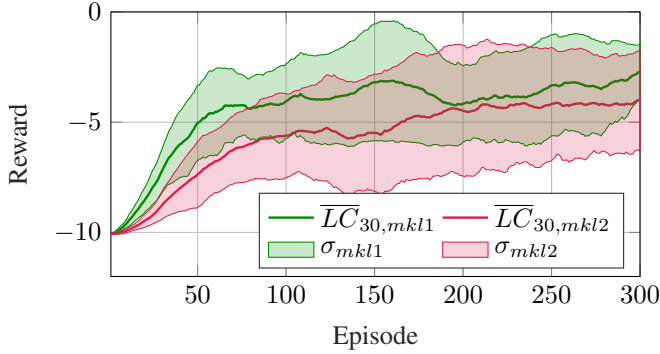


Fig. 12: Control with smaller mass.

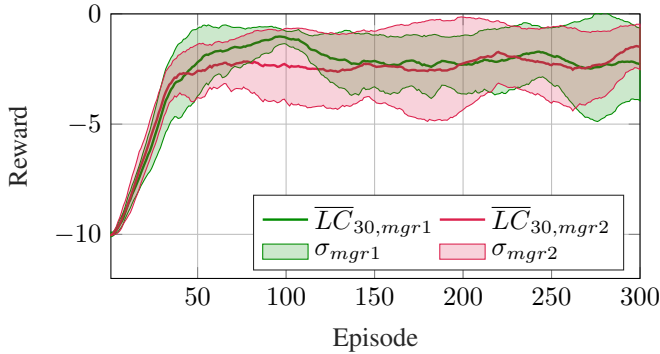


Fig. 13: Control with larger mass.

of the motor are simplified resulting in modelling error. The angular velocity \dot{u} is assumed to be constant and independent of m_2 . If the mass m_2 is reduced, for example, each action supplies less energy per time step to the system. Note that, especially in the initial swing-up phase, high energy supply is required to reach the desired energy level H_d as quickly as possible. However, a high mass in combination with the actions $a_1 = \text{'negative angle step'}$ and $a_2 = \text{'positive angle step'}$ can be challenging when stabilizing the desired energy level, which requires sensitive energy input. Thus, a trade-off between objectives arises.

In a first step, we reduce the mass m_2 to 1,5 kg (LC_{mkl1}) and in a second step to 1 kg (LC_{mkl2}) for the simulation. The simulation results are summarized in Fig. 12.

In comparison to the ICP-baseline, the achieved rewards are comparatively small and widely spreaded. In addition, the slope of the curves in the initial learning phase decreases with the reduction in mass. Resulting in an overall worse result caused by the poorer swinging capability of the second pendulum. Hence, the swing-up phase therefore requires more time. As a result, less reward is achieved which affects the mean value accordingly.

This is very different to the setup where the mass is, first increased to 3 kg (LC_{mgr1}) and then even further to 4 kg (LC_{mgr2}), as shown in Fig. 13.

It can be observed that the mean value curves are again in the same order of magnitude as the ICO-baseline. This is because the first pendulum gains more momentum from the movement of the second pendulum. At the same time,

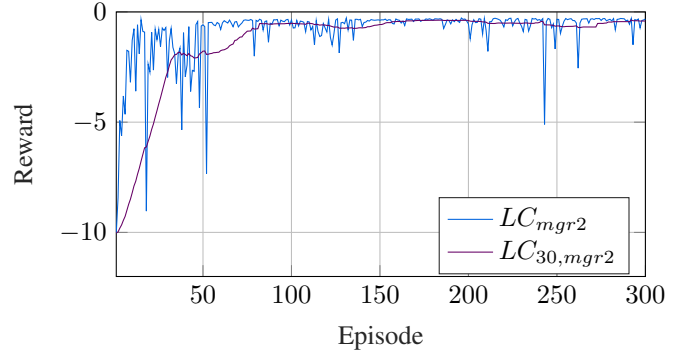


Fig. 14: Best learning curve obtained after doubling the mass.

the ability to stabilize the pendulum is slightly reduced. The initial learning phase ($< \text{episode } 50$) is also clearly visible. In addition, the difference between the case LC_{mgr1} and LC_{mgr2} is relatively small. The mass doubling also results in a very good learning curve, which is shown in Fig. 14.

We can observe that already after 50 episodes very high rewards are received. Apart from some peaks towards the end of the learning period, the learning curve is relatively smooth and the sliding average is very close to the zero target value.

Finally, we can conclude from the test scenarios above that the functionality of the RL algorithm seems to be independent from the mass. Moreover, the physical parameters, such as the mass or size of the angular steps, determine how high the rewards will be. This is because the RL algorithm de-facto only uses the means in order to achieve the desired target. Consequently, the mass, like other physical parameters, has to be chosen in such a way that it is compatible with the desired dynamical behaviour before the actual learning process is started.

VI. EXPERIMENTAL SETUP

In order to demonstrate the performance and robustness of our method, we deploy the proposed RL algorithm in an Acrobot experimental setup with limited computational resources. The setup is shown in Fig 1. We refer the reader to the accompanying video. The computations are conducted onboard a RaspberryPi 3B+ single board computer which is light enough to be mounted on the Acrobot's flywheel. Note that our RL algorithm is currently implemented in Python. We use a low-cost servo motor to drive the motion of the second pendulum. The Acrobot's angular position and velocity are determined based on the IMU data for which we choose a MPU-6050 GyS21 as a sensor. Because the gyroscope is prone to drift, we compensate the bias of current gyroscope reading based on the initial gyroscope reading. Moreover, we use a complementary filter in order to accurately determine the current angular position of the pendulum. The filtered measurements of the angular position θ and velocity $\dot{\theta}$ are then sent to the algorithm. The Acrobot is a rotary system. Hence, the power supply has to be realized on the flywheel which is done through standard USB-powerbanks. The overall mounting and wiring of the components is shown in Fig. 1. Note that all additional mountings have an impact on the

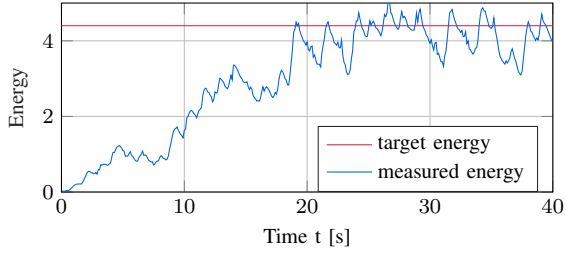


Fig. 15: Energy evolution in the 100th episode using the ICO.

Acrobot dynamics and posing additional challenges on the RL-algorithm.

We want to examine the performance for learning from scratch. Thus, no knowledge of the equation of motion is needed to apply the RL controller in the experiments. This makes the use of RL control especially appealing for deployment in scenarios which are complex to model.

We use the following initial configuration for the experimental setup (ICO_{exp}) in order to examine the performance and robustness of various setups:

Performance Baseline Setup ICO_{exp}

- We choose the same state space discretization as for the simulation in Sec. IV.
- The real experiments require much more time than the simulation. Therefore, the length of an episode is reduced to 40 s and the total learning time to 100 episodes. In contrast to simulation the real servo actuator requires time for positioning. Thus, we time step to $\Delta t_{\text{exp}} = 0.1$ s.
- Mass of the actuated pendulum is set up as stated in Tab. tab:params: tip mass $m_p = 0.038$ kg, rod mass $m_r = 0.042$ kg.
- Analogue to the simulation the algorithm can choose between two actions $a \in \mathcal{A} = \{a_1 = \text{'negative angle step'}, a_2 = \text{'positive angle step'}\}$. Thereby, we define the angle step as the maximal possible angle step which can be achieved by the servo motor in the time step $\Delta t_{\text{exp}} = 0.1$ s, applying the maximal available torque of the servo motor. Moreover, the angle u is restricted to the interval $[90^\circ, 270^\circ]$.
- For the experiments, the reward function from Eq. (7) is used. The desired energy level H_d is scaled in the experiment and is initialized by $\tilde{H}_d = 4,4$ Nm.

In order to ensure that the controller also learns well in the swing-up phase, a braking function is implemented since the system's damping is relatively small. For this, the second pendulum is used as an active damper in order to drive the first pendulum to its rest position. This allows the controller to begin the next episode from a stable rest position where $\tilde{H} \approx 0$. This drastically reduces the manual effort for collecting data.

In Fig. 15 an example of the energy curve after 100 episodes is shown for the proposed ICO_{exp}.

VII. EXPERIMENTAL RESULTS

In this section we present experimental results for the RL controller of the Acrobot for the case of energy stabilization at a desired level and for the control of rotation.

TABLE IV: Examined Acrobot configurations.

Case	Parameterization	# States $ \mathcal{S} $
ICO _{exp}	$\Delta\theta = 10^\circ, \Delta\dot{\theta} = 0.25$ rad/s	1441
C _{fine}	$\Delta\theta = 10^\circ, \Delta\dot{\theta} = 0.20$ rad/s	1801
C _{coarse}	$\Delta\theta = 20^\circ, \Delta\dot{\theta} = 0.25$ rad/s	721
C _{idle}	ICO with $\mathcal{A}_{\text{extended}} = \{a_1, a_2, a_{\text{idle}}\}$	1441
C _{long}	ICO with doubled episode length	1441
C _{mass}	ICO with increased pendulum mass m_p	1441

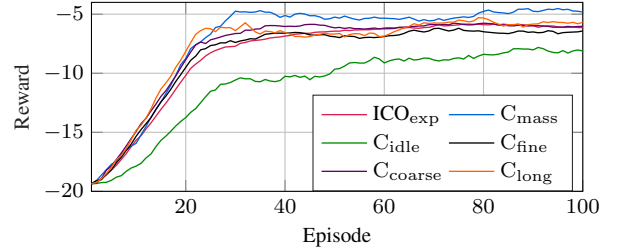


Fig. 16: Mean reward in the swing-up phase.

A. Energy Level Control

In the first part of this section we examine the RL controller's performance and robustness on energy level stabilization. For this, we analyze the influence of state space discretization, modification of the action space, the episode length, and the mass of the actuated pendulum on the performance of the RL controller in the experiment. As described in section V, we have run several simulations using modifications of the ICO from section IV beforehand, in order to figure out meaningful setups for our experimental study. This saves a significant amount of time, since learning in the simulation is much faster than in the experiment. It turned out for example, that good learning performance can also be achieved with the coarser discretization of the state space. Better results were achieved with twice the step size $\Delta\theta$. From these studies, we have chosen the best candidates for the set-up modifications in the experiment, which are summarized in the following.

In order to account for the performance of the RL controller in the swing-up phase and the hold phase, where the desired energy level has to be maintained, the corresponding learning curves are considered separately. Starting from results of the ICO_{exp} baseline as shown in Fig. 15, each episode is split into the time interval $[0, 20]$ s, which is the *swing-up* phase, and $[20, 40]$ s, which is the *hold* phase. This split results in two learning curves for each experimental run instead of one. In order to combine the information from two experiments, the mean value $\overline{LC}_{\text{exp}}$ of two independent learning-curves LC_{exp} is determined. This split allows for a more detailed analysis of the parameter influence.

The examined Acrobot configurations are summarized in Tab. IV. Using these configurations, the corresponding learning curves for the swing-up phase are shown in Figure 16.

As expected, with a larger pendulum mass C_{mass} the highest reward is generated. Consequently, the performance of the *swing-up control* of the first pendulum is best for the considered cases. Applying the coarse discretization C_{coarse}, the learning curve is steeper than that of the ICO_{exp}. Subsequently, they overlap and strive towards the same value. A doubled

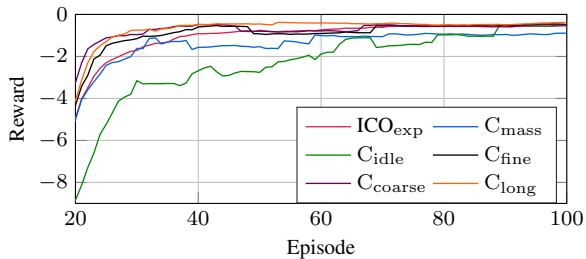


Fig. 17: Mean reward in the hold phase

episode length C_{long} leads to a lower reward for the same learning duration, as can be seen towards the end of the 50th episode. The same applies to the fine discretization C_{fine} . In addition, the worst performance during the swing-up was achieved when using the extended action space in case C_{idle} .

Analogue, the learning development during the *hold phase* is shown in Fig. 17. The stabilization performance decreases with increased pendulum mass C_{mass} . The use of longer episodes C_{long} leads to good results after only 50 episodes, which are at least as good as with the ICO_{exp} . Using the discretization cases C_{fine} and C_{coarse} , learning of the RL controller shows a better performance, as the learning curves are higher than the learning curve of the ICO_{exp} . However, towards the end of learning time they reach the same value, which means that the learning algorithm adapted well to the different situations. As far as the action space \mathcal{A}_3 is concerned, relatively many episodes pass until finally the level of the ICO_{exp} is reached.

Although using a greater mass results in higher reward during the swing-up phase, the hold phase reward is insensitive to the chosen set-up variations as they converge to almost the same reward values towards the end of the learning time. This can be clearly seen in Fig. 17, where many differences in the beginning of the learning period can be observed. The learning time is therefore well utilized by the RL algorithm, regardless of the studied different circumstances and setups. For the case of the doubled angular step size $\Delta\theta = 20^\circ$ in C_{coarse} learning is accelerated without noticeably affecting the control performance. As a result, this configuration seems promising direction for resource savings in future work.

Based on the previous results, we now examine combinations of the above setups to explore whether performance can be improved even further. Therefore, we combine the double angular increment C_{coarse} with longer episodes C_{long} , which both achieved promising results according Fig. 17. Moreover, we examine in a series of ten experimental cycles for the setup $C_{\text{coarse, long}}$ whether extending the action space by the *idle-action* a_{idle} has an influence on the performance. This experiment intended to show whether slow learning due to the idle action can be compensated with the advantages of double step size and longer episodes. In Fig. 18 and Fig. 19 the results for the swing-up phase and the hold phase are shown, respectively. The swing-up phase shows higher rewards when including action a_{idle} . However, by the end of the learning period, the controller received less overall reward compared to the ICO_{exp} . On the other hand, during the hold phase, the reward increase is steeper without a_{idle} . In conclusion,

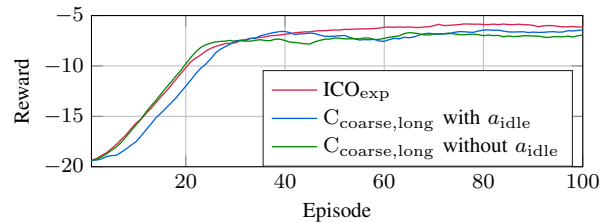


Fig. 18: Combined setup $C_{\text{coarse, long}}$ in the swing-up phase.

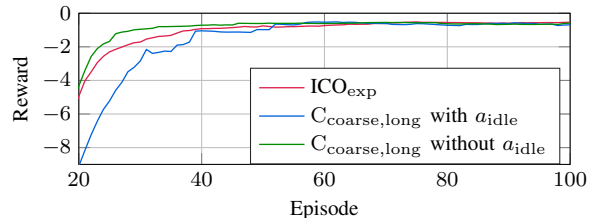


Fig. 19: Combined setup $C_{\text{coarse, long}}$ in the hold phase.

no clear advantage of the new combination with respect to the ICO_{exp} can be seen from either experiment, since no configuration shows best results for both, swing-up and hold phase, cf. Fig. 18 and 19 respectively.

As can be seen in Fig. 22, the corresponding value function qualitatively resembles the simulation results from Fig. 3, which validates the correct measurement of the angular position θ and velocity $\dot{\theta}$ of the first pendulum and the corresponding energy as given in Eq. (4). The scattered yellow dots in Fig. 22 represent states which were not visited up to episode 100. Thus, these states still possess their zero value from the initialization step. It turns out that the RL controller adapts well to different setups and achieves convergence to the desired control in all studied cases. In Fig. 20 and 21, the energy curve and the phase space trajectory of the first pendulum for the 100th episode are illustrated for the case $C_{\text{coarse, long}}$ without a_{idle} . Moreover, the average of ten

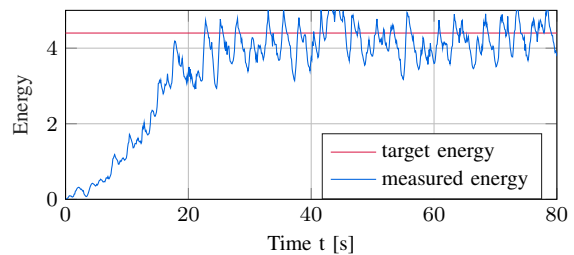


Fig. 20: Energy of the first pendulum in the 100th episode.

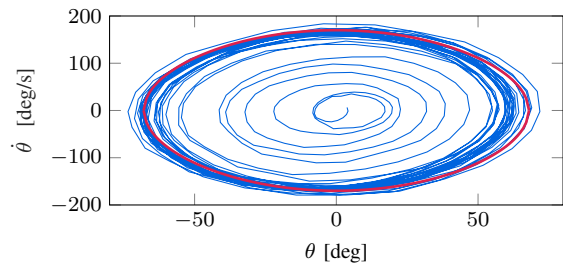


Fig. 21: Trajectory of the first pendulum in the 100th episode.

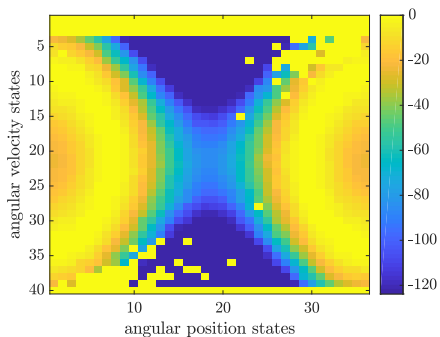


Fig. 22: State values after 100 episodes.

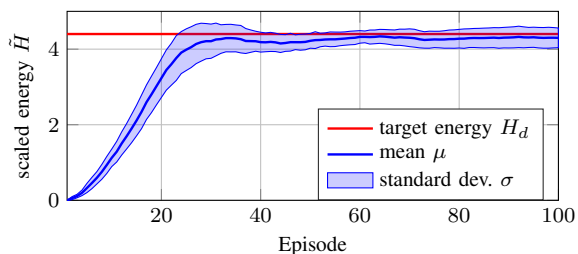


Fig. 23: Scaled energy \tilde{H} over 10 runs with $c_{\text{exp}} = 7.06$.

corresponding experimental runs shows that the mean energy converges quickly within the first 30 episode, see Fig. 23.

B. Rotation Control

In addition to energy control, further control goals can be considered by designing appropriate reward functions. Previously, we chose the energy level in a way such that the first pendulum does not reach the unstable equilibrium position at $\theta = 180^\circ$. In the following, we aim to drive the first pendulum towards a desired angular velocity during rotation. One possible approach is to enforce the rotation by setting a sufficiently large desired angular velocity. For this case $\tilde{H} > 2gc_{\text{exp}}$ has to be approximately fulfilled [16]. In the phase portrait, this corresponds to the area outside the separatrix, which is defined by $\tilde{H} = 2gc_{\text{exp}}$, so that the angular velocity $\dot{\theta}$ does not change its sign and the θ axis is not crossed in the phase space. The scaled Hamiltonian is only used at this point to approximate the required angular velocity. From Eq. (7) we get for the border case $\tilde{H} = 2gc_{\text{exp}}$ which separates the pendulum oscillation from the pendulum rotation

$$\dot{\theta} = \sqrt{4gc_{\text{exp}} \left(1 - \sin^2 \left(\frac{\theta}{2} \right) \right)}. \quad (13)$$

Thus, in this case the angular velocity has a maximum of $2\sqrt{gc_{\text{exp}}}$ and a minimum of zero. Note that the factor c_{exp} is not exactly known. Hence, we define $\dot{\theta}_d = 3\sqrt{gc_{\text{exp}}}$ as simplification. In addition, we reformulate the reward function as

$$R(\dot{\theta}) = -(\dot{\theta}_d - |\dot{\theta}|)^2. \quad (14)$$

Moreover, the state space domain for the RL controller has to be increased by doubling the width of the considered angular

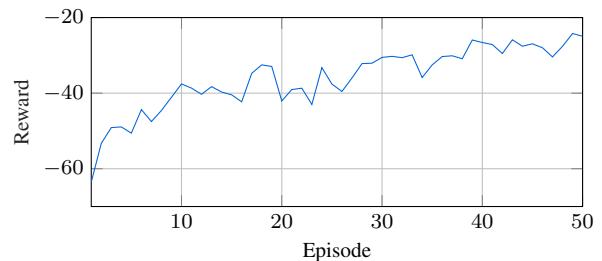


Fig. 24: Mean reward received after 20 s in each episode.

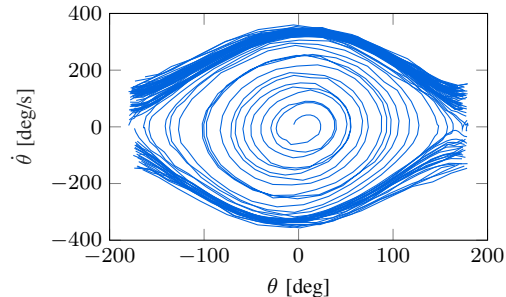


Fig. 25: Phase portrait for rotation control of the pendulum, as obtained in the experiment.

velocity interval to $[-10, 10]$ rad/s. The higher the desired angular velocity $\dot{\theta}_d$ is set, the more time is required for swing-up phase part of the episode. Therefore, we extend the episode length to 200 s and increase the mass m_2 for this experiment. Given the results from Sec. VII-A, we again double the step size to $\Delta\theta = 20^\circ$. Figure 24 depicts the average reward received in each episode after 20 s. The learning curve shows a clear upward trend. In order to accelerate the swing-up even more, the used action space $\mathcal{A}_{\text{extended}}$, see Tab. IV, is expected to improve the result even further. However, in this case the time step size would have to be at least tripled. This would have negative consequences for the determination of the exact state in the RL algorithm. In order to achieve higher angular velocities, longer episodes can be selected and the total learning time can be increased even further. Nevertheless the RL controller manages to bring the first pendulum into rotation with this configuration, as can be seen in the phase portrait depicted in Fig. 25 for the 50th episode.

The transitions between pendulum motion and rotational motion do not seem to cause any problems for the examined RL algorithm. Moreover, the state values are interpreted meaningfully in both operating ranges by the learning algorithm. This would be different if a classical control algorithm, such as for example sliding mode control, would be used, in which case the state space regions of different dynamical behavior would have to be known beforehand. This is not necessary if the presented RL control is used.

VIII. CONCLUSION AND FUTURE WORK

Results on RL control of an Acrobot in simulation and experiment are obtained in this study. Thereby the Acrobot is stabilized at a desired energy level. This energy level is given by the Hamiltonian of the first unactuated pendulum. Remarkably, the RL controller is capable of stabilizing the energy of the first pendulum close to the separatrix, which

separates the different dynamical regions of libration and rotation of the first pendulum. Although classical controllers, such as the sliding mode controller, can achieve a comparable performance as the RL controller, we have shown that there are crucial benefits if an RL controller is used. These benefits include that a knowledge of the underlined nonlinear dynamics is not necessary. Moreover, the RL controller adapts well to different phase space regions, such as the phase space regions of rotation and libration of the first unactuated pendulum of the Acrobot. It is also not necessary to develop different RL controllers for these distinct dynamics, as is the case in classical control design, where for example a swing up controller has to be developed. The presented experimental results demonstrate the feasibility to deploy the proposed RL algorithm on an Acrobot experimental setup using embedded architecture such as a RaspberryPi. The results show that the RL controller adapts well to different setups and achieves convergence to the desired control in all studied reasonable cases.

REFERENCES

- [1] M. W. Spong, "The swing up control problem for the acrobot," *IEEE control systems magazine*, vol. 15, no. 1, pp. 49–55, 1995.
- [2] V. Vaziri, A. Najdecka, and M. Wiercigroch, "Experimental control for initiating and maintaining rotation of parametric pendulum," *The European Physical Journal Special Topics*, vol. 223, no. 4, pp. 795–812, 2014.
- [3] P. Alevras, I. Brown, and D. Yurchenko, "Experimental investigation of a rotating parametric pendulum," *Nonlinear Dynamics*, vol. 81, no. 1-2, pp. 201–213, 2015.
- [4] L. Dostal, K. Korner, E. Kreuzer, and D. Yurchenko, "Pendulum energy converter excited by random loads," *Z. Angew. Math. Mech.*, vol. 98, no. 3, pp. 349–366, 2018.
- [5] S. C. Brown and K. M. Passino, "Intelligent control for an acrobot," *Journal of Intelligent and Robotic Systems*, vol. 18, no. 3, pp. 209–248, 1997.
- [6] J. Awrejcewicz, G. Wasilewski, G. Kudra, and S. Reshmin, "An experiment with swinging up a double pendulum using feedback control," *Journal of Computer and Systems Sciences International*, vol. 51, no. 2, pp. 176–182, 2012.
- [7] S. Lee, M. Eom, and D. Chwa, "Robust swing up and balancing control of the acrobot based on a disturbance observer," in *2015 15th International Conference on Control, Automation and Systems (ICCAS)*. IEEE, 2015, pp. 48–53.
- [8] L. Dostal and M.-A. PICK, "Theoretical and experimental study of a pendulum excited by random loads," *European Journal of Applied Mathematics*, vol. 30, no. 5, pp. 912–927, 2019.
- [9] C. Cyr, L. Dostal, D. A. Duecker, and E. Kreuzer, "Towards reinforcement learning-based control of an energy harvesting pendulum," in *2019 18th European Control Conference (ECC)*. IEEE, 2019, pp. 3934–3939.
- [10] "Restricted gradient-descent algorithm for value-function approximation in reinforcement learning," *Artificial Intelligence*, vol. 172, no. 4, pp. 454–482, 2008.
- [11] G. Boone, "Efficient reinforcement learning: Model-based acrobot control," in *Proceedings of International Conference on Robotics and Automation*, vol. 1. IEEE, 1997, pp. 229–234.
- [12] —, "Minimum-time control of the acrobot," in *Proceedings of International Conference on Robotics and Automation*, vol. 4. IEEE, 1997, pp. 3281–3287.
- [13] G. Brinkmann, W. M. Bessa, D.-A. Duecker, E. Kreuzer, and E. Solowjow, "Reinforcement learning of depth stabilization with a micro diving agent," in *2018 IEEE International Conference on Robotics and Automation (ICRA)*. IEEE, 2018, pp. 1–7.
- [14] R. S. Sutton and A. G. Barto, *Reinforcement learning: An introduction*. MIT press, 2018.
- [15] L. P. Kaelbling, M. L. Littman, and A. W. Moore, "Reinforcement learning: A survey," *Journal of artificial intelligence research*, vol. 4, pp. 237–285, 1996.
- [16] L. Dostal, K. Korner, E. Kreuzer, and D. Yurchenko, "Pendulum energy converter excited by random loads," *ZAMM-Journal of Applied Mathematics and Mechanics/Zeitschrift für Angewandte Mathematik und Mechanik*, vol. 98, no. 3, pp. 349–366, 2018.